GEOPHYSICAL RESEARCH LETTERS, VOL. 28, NO. 6, PAGES 1115-1118, MARCH 15, 2001

2D Hybrid simulations of the solar wind interaction with a small scale comet in high Mach number flows

M. W. Hopcroft and S. C. Chapman

Space and Astrophysics Group, University of Warwick, UK

Abstract. We investigate the structure and dynamics of the interaction between high Mach number solar wind flows and a cometary source that is "small scale" with respect to the cometary ion gyroscales, examples being Grigg-Skjellerup or P/Wirtanen. A series of 2D hybrid simulations are used and we focus on IMF orientations parallel and perpendicular to the simulation plane, these permit or prohibit propagation of modes with a component of $\underline{k}$ parallel to $\underline{B}_0$. The perpendicular cases show the onset of magnetosonic turbulence as M_A is increased; introducing a parallel $\underline{B}_0$ field component significantly changes this turbulence and the apparent shock structure seen on a 'fly-by'. This implies that the Alfvén-ion cyclotron mode plays a critical role in the observed structure, and we suggest the relevant mechanism must be resonant growth of such waves in the presence of magnetosonic turbulence from either the unstable ring beam distribution of the pickup ions, or shock reflected solar wind protons.

1. Introduction

The last twenty years have seen much effort directed towards observing and explaining the interaction of cometary ion sources in the supermagnetosonic flow of the solar wind (SW). This endeavour has ranged from extremely small scale "artificial comets" [*Valenzuela et al.*, 1986] to missions to Halley [*Gringauz et al.*, 1986], Giacobini-Zinner [*Von Rosenvinge et al.*, 1986], and Grigg-Skjellerup [*Johnstone et al.*, 1993]. Each of these differed in source rate and spatial extent, with corresponding differences in the structure observed. Although all exhibited some evidence of boundary layer crossings the details of the interactions were unique to each [*Mazelle et al.*, 1995; *Johnstone*, 1995]. Halley, with the largest neutral production rate of the three, affected SW plasma out to distances of $5 \times 10^6 km$ [*Gringauz et al.*, 1986], compared to a pickup ion gyroradius of $\sim 10^4 km$ [*Szegö*, 1988], and had several plasma boundaries, some open to interpretation. Grigg-Skjellerup represented the interaction at a much smaller source, and consequently was found to have fewer boundaries and a weaker shock-like interaction, such that on the inbound pass it was interpreted as a bow "wave" [*Coates et al.*, 1997].

Theoretical work has largely involved numerical simulations using MHD, hybrid, or two-fluid approaches. MHD codes have been used by [*Schmidt et al.*, 1993] and [*Murawski et al.*, 1998], and give information on global mass-momentum transfer, but are limited by their very nature to time and spatial scales in excess of ion gyroscales. For small scale sources, meaning that pickup ion trajectories are of the order of the interaction region as in this study, kinetic effects may play an important role. The smallest source studied, the AMPTE releases, have thus been modelled using hybrid techniques [*Delamere et al.*, 1999; *Chapman and Schwartz*, 1987]. Two-fluid simulations have been performed [*Sauer et al.*, 1996] which show a transition for extremely low production rates between cycloidal motion of heavy ions with superposed nonlinear structuring at low Mach numbers and less structuring at higher flow speeds, whereas a hybrid code was used by [*Lipatov et al.*, 1997] to investigate different source rates and interactions at moderately high, but fixed flow speeds. Their results showed increasing symmetry of the resultant structure, with low rates giving asymmetric test-particle like trajectories of the cometary pickup ions. Here we treat kinetic effects in the regime where the rate of mass production of cometary ions is sufficient to form a structure with a bow-wave/shock transition standing upstream of a core region dominated by those cometary ions, but with a halo of pickup ions permeating the shock itself. We are thus able to investigate the structure of "small scale" comets where the width of the region enclosed by the bow shock is of the order of the gyroradius of the pickup cometary ions. The interaction is between that of weakest comets where pickup ion motion dominates [*Bogdanov et al.*, 1996] and largest scale comets, such as Halley, where ion gyroscales are much smaller than the interaction region and hence which are admissable to MHD. We use a hybrid code to investigate in greater detail the shock structure of a fixed source rate in different Mach number flow which, we shall see, can generate significant structuring on scales between those of the SW proton and cometary ion pickup gyroradii.

2. Model

The equations solved in the code are the two ion kinetic equations of motion, Ampère's and Faraday's laws in the low frequency limit, and an equation resulting from electron momentum considerations for solving for the electric field. These are solved self-consistently under conditions of quasineutrality, zero electron inertia [*Chapman and Schwartz*, 1987] and constant electron pressure with the only source of resistivity being numerical. We represent spatial co-ordinates in 2D whilst resolving 3D fields, velocities and bulk plasma variables. For more details, see [*Terasawa et al.*, 1986].

We chose scaling for the simulations that essentially preserves the physics of interest whilst permitting calculations with good resolution both in configuration and velocity space. The interaction region length scale (L_{int}),

Paper number 2000GL000113.
0094-8276/01/2000GL000113$05.00

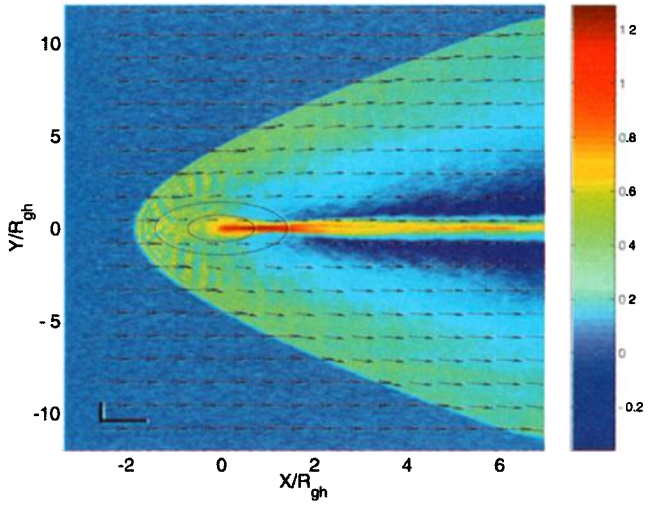

Plate 1. Total mass density ($\log_{10}$ scale) normalized to the unperturbed SW density, for a simulation with $\underline{B}_0$ in the plane and $M_A = 3.0$. The arrows show the bulk plasma flow direction and relative magnitude. The "circles" near the centre of the plot show the extent of the source regions described in the main text and the "L"-shape bottom left shows one cometary ion gyroradius in each direction to emphasize the scaling present. The axes are in units of cometary ion pickup gyroradii.

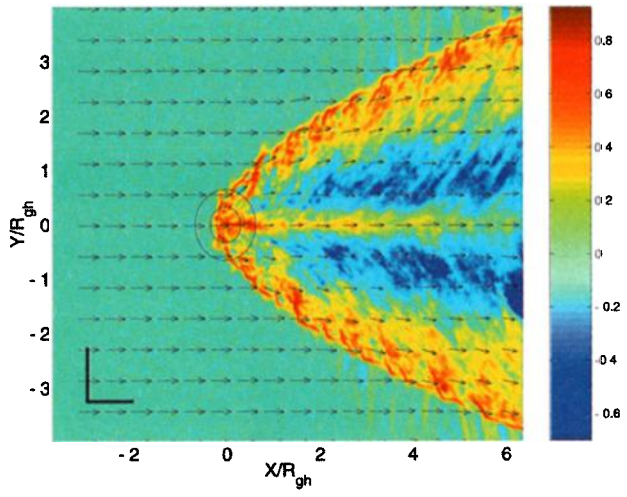

Plate 3. Total mass density ($\log_{10}$ scale) for a simulation with $\underline{B}_0$ in the plane and $M_A = 6.6$.

that is the region within the shock flanks, is scaled such that $L_{int} \sim R_{gh} > R_{gp}$, where the gyroradii $R_{gi} = \frac{v_{\perp i}}{\Omega_i}$ and $i = p, h$ refers to the protons and cometary source ions respectively. With $m_h = 4m_p$ we have scaling of $R_{gh}/R_{gp} \approx 78$ (fast flow with $M_A = 6.6$) and $R_{gh}/R_{gp} \approx 35$ (slow flow with $M_A = 3.0$) due to the difference between the heavy ion pickup velocity (that of the SW) and the much smaller thermal velocity of the protons. We also find $R_{gh}/L_{int} \approx 0.2$ (fast flow with $M_A = 6.6$). This compares to $R_{gh}/L_{int} \sim 0.08$ at Grigg-Skjellerup, with the encounter of ROSETTA with comet P/Wirtanen expected to give a larger ratio. A detailed comparison of neutral production rates is misleading when discussing a 2D simulation. Rather than generate the $(\frac{1}{r})$ ion distribution from a 2D (cylindrical) neutral source we use the $(\frac{1}{r^2})$ expected ion distribution in 3D. Our source region consists of a uniform inner core and a $\frac{1}{r^2}$ distributed outer halo producing 90% and 10% respectively, to represent a neutral source with a velocity distribution with a low energy thermal population and high energy tail. In our high Mach number flow simulations, this halo permeates the shock nose.

We use a CSE co-ordinate system with the simulation grid lying in the $x - y$ plane, and a computational domain of typically $-3R_{gh} < x < 6R_{gh}$. The upstream inflow boundary and downstream absorbing boundary permit flow through the simulation domain, the other boundaries are periodic. The grid cells are of size $dx = dy = 0.75\frac{v_A}{\Omega_p}$, with a grid typically containing 280×350 cells. Length is normalized to $\frac{v_A}{\Omega_p} \sim 0.04R_{gh} \sim 3R_{gp} \sim 55km$ with inflowing SW parameters of $B_0 = 18nT$, $n_p = 17cm^{-3}$, $v_{SW} = 630km/s$ (or $286km/s$ in plate 1) and $\beta_e = 0.27$, $\beta_p = 0.23$. We represent the proton population with 100 particles per cell. These conditions allow us to compare the effect of differ-

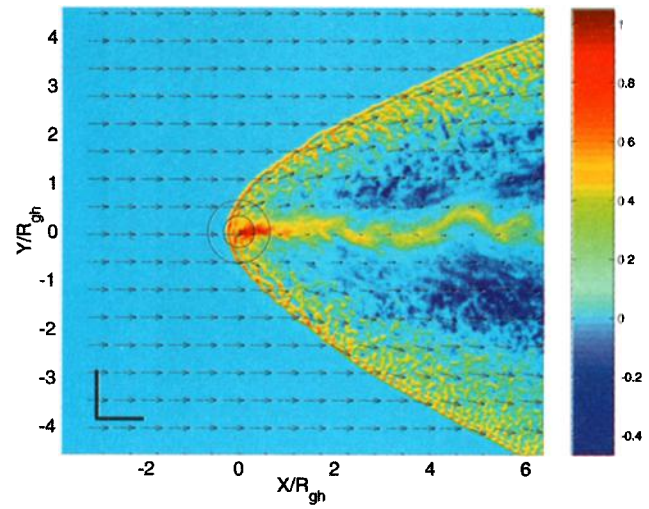

Plate 2. Total mass density ($\log_{10}$ scale) for a simulation with $\underline{B}_0$ perpendicular to the plane and $M_A = 6.6$.

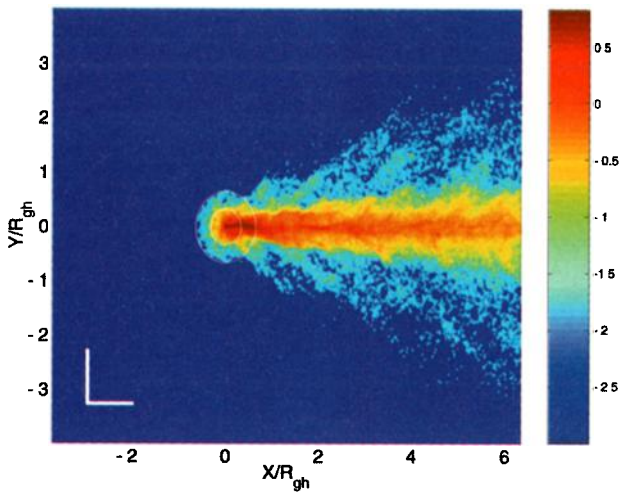

Plate 4. Mass density ($\log_{10}$ scale) of cometary ions only, for the same simulation as in plate 3.

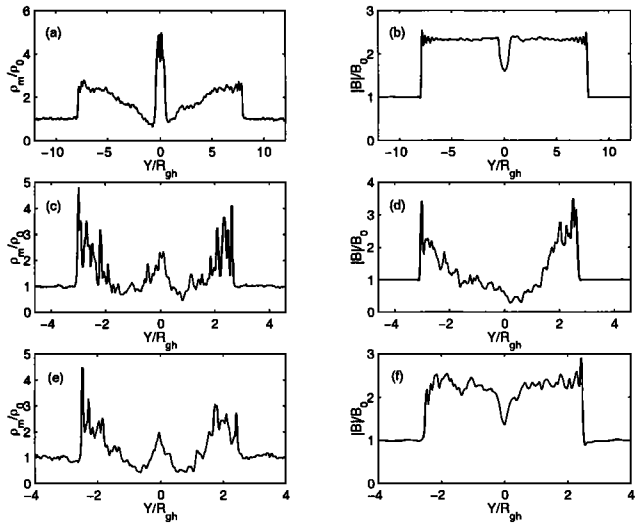

Figure 1. Cross-sections of total mass density and magnetic field magnitude at $x = 3R_{gh}$ downstream of the source. The top, middle and bottom panels refer to the simulations shown in plate 1 ($\underline{B}_0$ parallel to the simulation plane, $M_A = 3.0$), plate 2 ($\underline{B}_0$ perpendicular to the simulation plane, $M_A = 6.6$) and plate 3 ($\underline{B}_0$ parallel to the simulation plane, $M_A = 6.6$). Note length is normalized to R_{gh} and hence M_A.

ent SW flow speed as a comet approaches the Sun or passes through a fast flowing region of SW plasma.

3. Results

The simulations are evolved from an initial condition of uniform SW plasma. Cometary ions are added until the simulation has evolved to a steady-state, verified by checking that the total of both protons and cometary ions in the simulation box is roughly constant in time.

The IMF is in all cases perpendicular to the SW flow velocity, in common with most fly-by conditions. We first summarize the structure at a relatively low SW Mach number, $v_{SW} = 3v_A$ ($M_{MS} = 2.75$). Plate 1 shows a colour contour of the combined mass density (both SW protons and cometary ions) across the simulation grid. Here the IMF is in the y-direction (in the simulation plane) and the "L"-shape in the bottom left corner of each plot highlights one cometary ion gyroradius in each direction. The concentric "circles" near the centre mark the outer boundaries of the two cometary mass loading regions (the ellipsoidal shape of these regions is due to different scaling of the x & y axes). Plate 1 conveniently displays three regions of interest. The first, the shock front, is clearly visible as a jump in density and also exhibits a deflection and reduction in magnitude of the bulk plasma flow. A high density plasma tail stretches from the centre of the source region directly downstream to the absorbing boundary. Finally, low density lobes can be seen either side of the tail. The shock jump is well defined and steady as is essentially that produced for simulations at the same flow speed with the IMF perpendicular to the plane (not shown): it is the expected magnetosonic shock jump.

We now increase the SW Alfvén Mach number to $M_A = 6.6$ ($M_{MS} = 6.04$). Plate 2 shows a similar plot, but for a simulation with the IMF perpendicular to the plane at this higher flow speed. With this IMF orientation, Alfvén-ion cyclotron and whistler waves cannot propagate in the simulation so we see the behaviour of magnetosonic waves only. The increase in Mach number of the flow has introduced magnetosonic turbulence downstream of the shock, although the shock jump is still well defined. We also see Kelvin-Helmholtz instability in the cometary ion tail as this is no longer stabilized by field line draping in this orientation, and an asymmetry of the entire structure due to momentum transfer perpendicular to the flow direction (see e.g. [*Chapman and Dunlop*, 1986; *Chapman and Schwartz*, 1987; *Delamere et al.*, 1999]).

We now 'switch on' wavemodes propagating with components of $\underline{k}$ parallel to the magnetic field in addition to magnetosonic modes by performing a simulation (shown in plate 3) with the field in the plane of the simulation (the IMF is in the y-direction). Field line draping occurs, with maximum field pile up (not shown) occuring near the centre of the source region and the Kelvin-Helmholtz instability in the tail is now stabilized. The shock turbulence is significantly different to that in the previous plot found for magnetosonic waves only. The structuring is at longer wavelengths, on length scales between R_{gp} and R_{gh} and is seen in the deflected flow layer immediately behind the shock and on deep into the lobes. The shock also generates whistler waves which can be seen travelling upstream of the shock flanks. By varying the cell size we have verified that the turbulence length scale is not affected by the choice of grid. A comparison with plate 4, which shows the mass density of only the cometary ions for the same simulation, reveals that only the "nose" of the shock is populated by a mixture of both SW protons and cometary ions. The core of the source region provides the main obstacle to SW flow whilst the halo permeates the shock front, allowing some heavy ion pickup in faster flow. Sufficiently far along the flanks of the shock there are protons only. The structure in proton density along the flanks can thus be seen to differ from that observed in [*Bogdanov et al.*, 1996] as there are no heavy ions present in this region and hence the protons are not merely reacting to local structure in the heavy ions. From this we conclude that the turbulence is either generated at the nose of the shock from the free energy of pickup cometary ions and then propagates along the flanks, or arises locally from the free energy of shock reflected protons.

We can obtain a crude comparison with cometary fly-by data by plotting cross- sections (of total mass density and $|\underline{B}|$) and these are shown in figure 1. At low Mach number flow (top panel) the shock transition is well defined and remains so in fast Mach number flow with the field perpendicular to the simulation (middle panel), with magnetosonic turbulence introduced downstream of the shock. With the field in the plane (bottom panel) the left and right side shock transitions appear to be less similar — a consequence of the larger scale on which fluctuations now occur.

4. Summary

The interaction between fast SW flow ($M_A = 6.6$, $M_{MS} = 6.04$) and a "small scale" cometary ion source, that is, with cometary ion gyroscales of the order of the interaction region, have been investigated with 2D hybrid simulations. At low Mach number SW flow ($M_A = 3.0, M_{MS} = 2.75$) the cometary structure generally, and the shock transition in particular, are smooth. The IMF can be oriented

perpendicular or parallel to the simulation plane to prohibit or permit propagation of waves with a component of $\underline{k}$ along $\underline{B}_0$. At high flow speeds ($M_A = 6.6, M_{MS} = 6.04$) with $\underline{B}_0$ perpendicular to the simulation plane we generate magnetosonic turbulence behind the (still well defined) shock. With $\underline{B}_0$ in the simulation plane, the character of the turbulence changes, the shock jump is less well defined and the fluctuations have larger characteristic spatial scales. Importantly, these turbulent structures appear throughout the shock region, both in the nose which is populated by cometary pickup ions, and in the flanks where no cometary ions are present. This implies that:

1. The turbulence is associated with parallel or oblique modes such as Alfvén-ion cyclotron waves.
2. It evolves in the presence of magnetosonic turbulence.
3. Free energy is available from ring beam distributions of cometary pickup ions in the shock nose and, to a lesser extent, reflected SW protons throughout the shock.

A possible explanation is the resonant growth of ion cyclotron waves in the presence of magnetosonic turbulence as in [*Winske and Gary*, 1986]. The most significant source of free energy is the ring beam distribution of cometary pickup ions, the waves then simply propagating to the shock flanks, although in principle local generation with the protons is a possibility. Since the frequency of the fastest growing mode will depend on the (here strongly varying) beam density we are unable to extract a characteristic frequency from our simulations, the restricted spectral analysis that is possible shows that the turbulence is broadband.

Acknowledgments. This work was supported by EPSRC, PPARC and HEFCE. Calculations were carried out using the high performance computing facility GRAND.

References

Bogdanov A. *et al.*, Plasma structures at weakly outgassing comets–results from bi-ion fluid analysis, *Planet. Space Sci., 44*, (6), 519–528, 1996.

Chapman S. C. and M. W. Dunlop, Ordering of momentum transfer along $\underline{V} \times \underline{B}$ in the AMPTE solar wind releases, *J. Geophys. Res., 91*, 8051–8055, 1986.

Chapman S. C. and S. J. Schwartz, One-dimensional hybrid simulations of boundary layer processes in the AMPTE solar wind Lithium releases, *J. Geophys. Res., 92*, 11059–11073, 1987.

Coates A. J. *et al.*, Bow shock analysis at comets Halley and Grigg-Skjellerup, *J. Geophys. Res., 102*, 7105–7113, 1997.

Delamere P. A. *et al.*, A three-dimensional hybrid code simulation of the December 1984 solar wind AMPTE release, *Geophys. Res. Lett., 26*, 2837–2840, 1999.

Gringauz K. I. *et al.*, First *in situ* plasma and neutral gas measurements at comet Halley, *and others in this issue, Nature, 321*, 282–285, 1986.

Johnstone A. D., Cometary ion pickup processes: Halley and Grigg-Skjellerup compared, *Adv. Space Res., 16*, (4), 11–18, 1995.

Johnstone A. D. *et al.*, Observations of the solar wind and cometary ions during the encounter between Giotto and P/Grigg-Skjellerup, *Astron. Astrophys., 273*, (1), 1–4, 1993.

Lipatov A. S. *et al.*, 2.5D hybrid code simulation of the solar wind interaction with weak comets and related objects, *Adv. Space Res., 20*, (2), 279–282, 1997.

Mazelle C. *et al.*, Comparison of the main magnetic and plasma features in the environments of comets Grigg-Skjellerup and Halley, *Adv. Space Res., 16*, (4), 41–45, 1995.

Murawski K. *et al.*, Two-dimensional MHD simulations of the solar wind interaction with comet Halley, *Acta Astron., 48*, 803–817, 1998.

Sauer K. *et al.*, Bi-ion discontinuities at weak solar wind mass-loading, *Physica Scripta, T63*, 111–118, 1996.

Schmidt H. U. *et al.*, MHD modelling applied to Giotto encounter with comet P/Grigg-Skjellerup, *J. Geophys. Res., 98*, 21009–21016, 1993.

Szegö K., Modelling a cometary nucleus, *Astrophys. Space Sci., 144*, 439–449, 1988.

Terasawa T. *et al.*, Decay instability of finite-amplitude circularly polarized Alfvén waves – a numerical simulation of stimulated Brillouin scattering, *J. Geophys. Res., 91*, 4171–4187, 1986.

Valenzuela A. *et al.*, The AMPTE artificial comet experiments, *Nature, 320*, (6064), 700–723, 1986.

Von Rosenvinge T. T. *et al.*, The international cometary explorer mission to comet Giacobini-Zinner, *and others in this issue, Science, 232*, 353–356, 1986.

Winske D. and S. P. Gary, Electromagnetic instabilities driven by cool heavy ion beams, *J. Geophys. Res., 91*, 6825–6832, 1986.

M. W. Hopcroft and S. C. Chapman, Space and Astrophysics Group, University of Warwick, Coventry, CV4 7AL, UK. (email: hopcroft@astro.warwick.ac.uk)

(Received May 16, 2000; revised August 17, 2000; accepted September 22, 2000.)